Dynamic Optimization of Electric Arc Furnace Operation

Richard D. M. MacRosty and Christopher L. E. Swartz
Department of Chemical Engineering, McMaster University, 1280 Main Street West, Hamilton, Ontario, Canada L8S 4L7

DOI 10.1002/aic.11104
Published online February 5, 2007 in Wiley InterScience (www.interscience.wiley.com).

The main objective of this work is the development of a computational procedure for determining optimal operating strategies for an industrial electric arc furnace (EAF). These goals are achieved by incorporating a detailed mechanistic model into a mathematical optimization framework. The model used in this work includes mass and energy balances, and contains sufficient detail to describe the melting process, chemical changes, and material and energy flows. Mathematical optimization is used to determine the optimal input trajectories based on an economic criterion; process limitations are accounted for by including them within the optimization problem as constraints. This optimization procedure considers trade-offs between all the process inputs and processing time, so as to maximize the profit. Several case studies illustrating the use of mathematical optimization in the enhancement of process performance are given. © 2007 American Institute of Chemical Engineers *AIChE J,* 53: 640–653, 2007
Keywords: electric arc furnace, EAF, dynamic model, process optimization, dynamic optimization

Introduction

Electric arc furnaces (EAFs) are widely used in the steel industry for recycling scrap steel by melting it down and adjusting the chemistry to obtain the desired product grade. Melting the steel is achieved using both chemical and electrical energy sources. Electrical energy is added to the steel charge by multiple electrodes; the high-voltage developed between the electrodes and the scrap steel induces an electric arc to develop from the tip of the electrode to the scrap steel. The energy from the arc is transferred to the steel directly through resistance heating and also radiative heating. The chemical contribution is derived from combustion reactions taking place in the furnace, fuelled predominantly by coke, natural gas and oxygen additions. In the steel industry EAFs are run in batches, termed heats. While processing conditions vary greatly, a typical heat takes between one to three hours, and consumes 400 kWh/ton of steel.[1] Irons[2] indicates that modern furnaces are now consuming less than 300 kWh/ton of electrical energy. The lower dependence on electrical power is a result of operational improvements and also due to a greater reliance on energy derived from chemical sources. The energy-intensive nature of EAFs make these operations attractive candidates for optimization.

The EAF process operation begins with charging scrap steel into the furnace. Depending on the operation, a single charge could be in the region of 100 tons. The scrap is preheated with burners fuelled by a mixture of natural gas and oxygen. Once it is deemed that no further benefits can be gained from the burners alone, the electrodes are lowered and the power is turned on. Initially, the transformer voltage tap is kept at a low setting due to instability when arcing to solid scrap. As the pool of liquid forming at the base of the arc grows, the voltage setting, and, hence, power level, can be increased. Once sufficient scrap has melted, a second or even a third scrap charge may be added to the furnace. Subsequent charges are typically

Current affliation of R. D. M. MacRosty: Hatch Ltd, 2800 Speakman Drive, Sheridan Science & Technology Park, Mississauga, Ontario, Canada L5K 2R7.
Correspondence concerning this article should be addressed to C. Swartz at swartzc@mcmaster.ca.

smaller than the initial charge. During the operation, lime is added to the bath to improve foaming properties of the slag. Oxygen and carbon are also injected into the bath to encourage foaming and manipulate the bath chemistry. Foaming is desirable since it protects the furnace walls from radiation, and improves efficiency by increasing the percentage of energy transferred into the bath while decreasing radiation losses from the bath. Once the bath reaches the desired temperature and composition, the furnace is tapped; meaning the molten steel is drained from the furnace. It is common practice to leave some of the molten steel in the furnace as a "hot heel" to aid in preheating the subsequent batch.

With the exception of power regulation, EAFs typically involve a relatively low-level of automation, and rely heavily on operator intuition. As with most industrial processes, operator experience is invaluable for the operation of the process. However, this experience-based knowledge can be limited due to the complex multivariable interactions and subtle relationships occuring during processing. The understanding of these complexities is confounded by the small number of useful process measurements, making it difficult to infer the current state of the process. Therefore, in most situations, process operating procedures are recipe-based, determined from what has worked well in the past, and process improvement is often achieved through adjustment of process inputs for future batches based on past operation.

The manner in which reagents, scrap and electrical power are added to the furnace may be carried out in multiple ways. Detailed process knowledge, in the form of a model, makes it possible to understand the more complex relationships and evaluate different operating strategies. Furthermore, the model enables process experimentation to be carried out without the possibility of economic risk or the occurrence of dangerous events. Several such simulation studies may be carried out, testing possible input profiles over a wide range of conditions and evaluating a performance criterion. While this approach to process optimization is simple and intuitive, the extent to which the search space is investigated is severely limited, and even finding solutions where variables remain feasible can be challenging. A more systematic approach is to pose and solve the problem within a mathematical optimization framework.

Woodside et al.[3] use optimal control theory to determine the optimal power trajectory during the carbon-injection stage of the EAF steelmaking process. The objectives are to minimize power and duration subject to endpoint constraints on temperature and carbon content, as well as path constraints. The model used by the authors contains two physical states: carbon reacted and temperature. The authors apply the steepest descent method, as well as an approach that seeks to directly satisfy the necessary conditions for optimality as given by Pontryagin's maximum principle.

Gosiewski and Wierzbicki[4] consider the melting stage of an EAF operation, and use a simple, single state model that relates the power input to the bath temperature. The manipulated variables are the transformer tap and the arc current; the authors assume that the transformer tap would be kept at its maximum and thus only consider the manipulation of the current. An economic objective comprising of the cost of power and the time of operation is maximized using Pontryagin's maximum principle.

Görtler and Jörgl[5] develop a supervisory control system for an industrial furnace that uses a fuzzy logic model to relate the arc radiation to the water cooled panel temperatures of the furnace walls and roof. The control objective is to maximize meltdown power without overly stressing the vessel walls by using the transformer tap and impedance setpoints as manipulated variables. Rigorous mathematical optimization is not applied.

Oosthuizen et al.[6] investigate the application of model predictive control (MPC) to EAF operation, where the controller tuning parameters are based on economic considerations. MPC involves optimization of manipulated input trajectories at each sampling period; in this case with a linear dynamic model and quadratic cost function. In their study, the economic impacts of deviations from the setpoints are based largely on heuristics, and the setpoints themselves are not determined by optimization.

Boemer and Roedl[7] investigate the influence of lancing conditions and the electric arc on the fluid dynamics of an electric arc furnace. Performance measures relative to the current operation are evaluated through physical tests carried out on an experimental rig and numerical simulation.

Pozzi et al.[8] discuss a system that has been developed that uses offgas chemistry data to update their model and control combustion in the freeboard by manipulating the burner flow; however, no details of the model or mechanisms to determine inputs are provided. Other industrial studies[9,10] analyze process data with the goal of predicting improved operational policies; while optimization is referred to, the rigor to which it is applied is unclear.

Much of the work carried out on EAF optimization tends to be on either highly simplified models or on models that consider only isolated aspects of the furnace. A drawback of these studies is that by optimizing one of the subprocesses of furnace operation, other subprocesses may be negatively impacted. To ensure that the optimal operation of the furnace is achieved, it is necessary to consider all the subprocesses in the furnace simultaneously. An excellent example of this approach available in the published literature is the work by Matson and Ramirez.[11] They develop a first-principles based model, and use iterative dynamic programming to solve the resulting dynamic optimization problem. The model approximates the furnace as two separate control volumes in which chemical equilibrium is assumed. The input variables included in the optimization problem are the carbon injection, oxygen lancing, burner O_2 and the batch duration. The authors use a weighted objective function to minimize the amount of CO in the offgas, the final amount of FeO and the batch duration. A penalty function is also included in the objective function to penalize the bath temperature if it falls below 1,920K (coinciding with the end of the melt).

In this paper, a comprehensive model of electric arc furnace operation developed by MacRosty and Swartz[12] is used within a rigorous dynamic optimization framework. An economic objective function is optimized, subject to endpoint and path constraints. The optimization problem formulation and implementation are described, and its performance illustrated through several case studies. This paper is structured as follows. A summary of key approaches for the optimization of differential-algebraic equation (DAE) systems is presented, followed by an overview of the furnace model. The formulation of the

optimization problem is then given, followed by a discussion of implementation considerations, and a series of case studies that illustrate the application of the optimization approach. This article concludes with a summary and discussion.

Optimization of Differential-Algebraic Equation Systems

To capture the dynamics of the EAF process, it has been modelled as a differential-algebraic equation (DAE) system. Differential variables, also known as differential states, are time dependent, and may be a function of the external forcing functions, other state variables, algebraic variables and time. DAE systems are more challenging to solve than purely algebraic systems due to the presence of the differential states that must be integrated, and the infinite-dimensional search space of the decision variables. We consider here the following general formulation for dynamic optimization of differential-algebraic equation systems, based on that given in Cervantes and Biegler.[13]

$$\min \quad \varphi(\mathbf{x}(t_f), \mathbf{z}(t_f), \mathbf{u}(t_f), t_f, \mathbf{p}) \tag{1}$$

s.t.

$$\frac{d\mathbf{x}(t)}{dt} = \mathbf{f}(\mathbf{x}(t), \mathbf{z}(t), \mathbf{u}(t), t, \mathbf{p}) \tag{2}$$

$$\mathbf{0} = \mathbf{h}(\mathbf{x}(t), \mathbf{z}(t), \mathbf{u}(t), t, \mathbf{p}) \tag{3}$$

$$\mathbf{0} \geq \mathbf{g}(\mathbf{x}(t), \mathbf{z}(t), \mathbf{u}(t), t, \mathbf{p}) \tag{4}$$

$$\mathbf{0} \geq \mathbf{g}_s(\mathbf{x}(t_s), \mathbf{z}(t_s), \mathbf{u}(t_s), t_s, \mathbf{p}) \tag{5}$$

$$\mathbf{x}(0) = \mathbf{x}_0 \tag{6}$$

where, $\mathbf{x}(t)$ is a vector of differential states; $\mathbf{z}(t)$ is a vector of algebraic states; $\mathbf{u}(t)$ is a vector of control inputs; $\mathbf{p}$ is a vector to time-independent parameters; $\mathbf{f}$ are differential equation constraints; $\mathbf{h}$ are algebraic equation constraints; $\mathbf{g}$ are path inequality constraints; $\mathbf{g}_s$ are point constraints at specific times t_s; t_f is the final time.

The objective function, Eq. 1, is typically formulated to represent a performance measure of the system, such as the economic cost or the integral square error from a desired value. The model equations are included as constraints; Eqs. 2 and 3 represent the differential and algebraic model equations, respectively. The general path constraints, Eq. 4, may include simple bounds on time-dependent variables.

A variety of sophisticated techniques have been developed for the optimization of problems involving DAEs. Variational or indirect methods, which make use of the first-order necessary conditions obtained from Pontryagin's maximum principle[14] to locate the optimum, have had limited success with large-scale realistic problems. Methods which discretize the continuous-time problem to obtain a finite-dimensional problem have been more successful; Biegler and Grossmann[15] categorize these methods as partial or complete discretization, based on the level of discretization implemented in the formulation of the problem. In these direct methods, the control inputs are typically represented as piecewise polynomials whose coefficients are included in the search space.

Complete discretization methods discretize the state profiles in addition to parametrization of the inputs, using a technique, such as orthogonal collocation on finite elements[16] to approximate them as piecewise polynomials. Typically, Lagrange interpolation polynomials are used since the coefficients of these polynomials correspond to the value of the states at the collocation points. This property allows meaningful bounds to be implemented directly in the formulation. The DAE system is converted to a purely algebraic system, which may then be included as algebraic constraints in a conventional nonlinear programming (NLP) problem in which the integration and optimization are in effect carried out simultaneously. A drawback of this method is that the resulting NLP problem can be very large, and it may be necessary to sacrifice accuracy through use of a coarse discretization of input and state profiles in order to obtain a computationally tractable problem. Initialization of the state variable profiles is also required. Strategies for improving the computational efficiency include reduced space sequential quadratic programming (rSQP) techniques,[17] and use of interior-point optimization[18] as an alternative to active-set strategies. Hong et al.[19] propose a sequential solution approach in which the algebraic equations representing the discretized DAE system are solved as a subsystem at each optimization iteration. The smaller dimension of the optimization problem has to be weighed against the requirement for repeated solution of the model equations, but could be beneficial for certain types of problems.

Partial-discretization methods involve the discretization of only the control variables. A sequential-solution strategy involves successive execution of optimization and integration steps.[20] Gradient information, for the optimization step, is obtained through finite-difference perturbations, integration of the adjoint equations or the integration of the sensitivity equations, and is then passed to a nonlinear programming (NLP) solver, which determines how to manipulate the control input parameters as it iterates to find the optimum. This is considered a feasible-path method since the integration is carried out at each iteration, as opposed to the simultaneous approach, where the integration is effectively carried out only at the final solution. Disadvantages of the sequential method are that the integration at each iteration is expensive, which accounts for a substantial part of the computational time, and this method is not suited for use with problems with unstable modes due to the method's reliance on obtaining the solution of an initial value problem at each iteration.

Multiple shooting[21–23] is another method in which the optimization and integration are decoupled. The time horizon is partitioned, and the DAE system integrated over each time interval. The initial values corresponding to each interval are included as optimization variables, and continuity of the states included as equality constraints at the optimization level. This method is consequently both sequential and simultaneous in character.

Dynamic programming is based on Bellman's principle of optimality,[24,25] and does not involve solution of an NLP directly. However, its application to large-scale problems has had limited success due to the computational expense associated with the solution of these problems.

Both complete and partial discretization methods have been successfully employed on a large range of different problems. The sequential approach was used in this work, as implemented in gPROMS/gOPT.[26] However, recent develop-

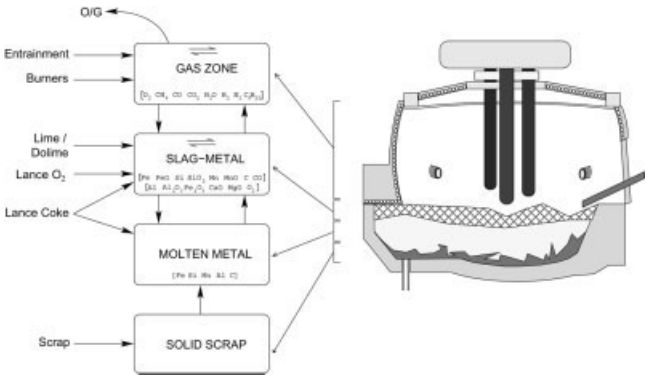

Figure 1. EAF model.

ments by Biegler and coworkers[17,18] suggest that either method could be viable for this process.

Model Overview

The model used in this work is a comprehensive nonlinear-dynamic model developed from fundamental mass and energy-balance relationships. A degree of empiricism was introduced to model aspects of the process where the mechanisms are not well understood. An overview of the model is presented here; the detailed mathematical model is presented elsewhere.[12]

The EAF model is divided into four zones: the gas zone, the slag-metal interaction zone, the molten-steel zone and the solid-scrap zone. The gas zone is assumed to be in a state of chemical equilibrium that includes all gas in the freeboard volume, that is the free space in the furnace above the scrap material. The slag-metal interaction zone includes all the slag material and the portion of iron interacting with the slag, and is also in a state of chemical equilibrium. The chemical equilibrium assumption in the slag-metal interaction and the gas zones is reasonable if one considers the high-temperatures within the system.[1,27] The molten-steel zone consists of all metallic elements in their liquid state excluding that portion included in the slag-metal zone. The solid-scrap zone includes the charged scrap that is still in solid form. All reactions are assumed to occur in the gas and slag, and, thus, no reactions are considered in the molten steel or solid-scrap zones. The reaction of material is limited by mass transfer between the zones, where the mass-transfer coefficients are treated as parameters and are estimated from industrial process data. Figure 1 is a diagram of the model, depicting the mass flows between the above described zones. The chemical species included in each zone and the material additions are also illustrated. The energy model considers the radiation and convective heat transfer taking place between different zones, the furnace elements and the arc. The model has sufficient detail to account for the effects of the foaming slag on power transfer from the arc to the steel.

The material flows in each zone are tracked with an atom balance

$$\frac{d}{dt}(b_{k,z}) = F_{k,z}^{in} - F_{k,z}^{out} \tag{7}$$

where b_k is the molar abundance of element k and F_k^{in} and F_k^{out} are the inward and outward flows of element k respectively. The chemical equilibrium for this multireaction system can be computed by minimizing the Gibbs-free energy. The method used in the model does not require reaction stoichiometry to compute equilibrium. Instead, it includes the system of equations obtained from the first order necessary conditions for constrained minimization of the Gibbs free energy

$$\sum_i n_i^* a_{ik} = b_k \tag{8}$$

$$\Delta G_{f,i}^o + RT \ln \hat{a}_i + \sum_k \lambda_k a_{ik} = 0 \tag{9}$$

where n_i^* is the moles of species i at equilibrium in the specified zone; a_{ik} is the number of atoms of k in species i: b_k is the number of moles of element k; $\Delta G_{f,i}^o$ is the Gibbs free-energy of formation; $\hat{a_i}$ is the activity of species i and is a function of the system composition, temperature and pressure; and λ_k are Lagrange multipliers. A useful property is that the chemical equilibrium problem is convex when not combined with phase equilibrium problem.[28]

The following energy balance was implemented for each zone

$$\frac{d}{dt}(E_z) = Q_z + \sum_{i=1}^{n} F_{i,z} H_{i,z}\bigg|_{in} - \sum_{i=1}^{n} F_{i,z} H_{i,z}\bigg|_{out} \tag{10}$$

where Q_z is the heat flow added to zone z; $F_{i,z}$ is the molar flow of component i to/from zone z and $H_{i,z}$ is the corresponding enthalpy. The flows are given in terms of the compounds and relate to elemental flows described in Eq. 7 by: $F_{k,z} = \Sigma_i a_{ik} F_{i,z}$, where k refers to the element and i to the compound. The energy holdup at any time is computed as

$$E_z = \sum_{i=1}^{n} n_{i,z}^* H_{i,z} \tag{11}$$

A more complete description of each of the four zones follows:

Gas Zone: The gas zone includes all material in the freeboard volume. The species considered in this zone are: CO, O_2, CO_2, CH_4, H_2, H_2O, N_2 and C_9H_{20}. C_9H_{20} is taken to be an average composition of all the volatile components that may be present in the scrap, and is assumed to vaporize from the slag in the initial minutes of charging. CH_4 and O_2 are added to this zone via the burners. O_2, N_2 and H_2O are introduced from air ingress and water-cooling at the electrodes, while CO enters from the partial combustion of carbon in the slag-metal interaction zone. The components within this phase are assumed to exist in a state of chemical equilibrium.

Slag-Metal Interaction Zone: This zone consists of the slag material and a portion of the molten-metal phase with which it is in contact, including metal droplets in the slag. The species considered in this zone are: Fe, Mn, Mg, Al, Si, FeO, Fe_2O_3, MnO, MgO, Al_2O_3, SiO_2, CaO, C, CO, O_2, N_2. This zone is in direct contact with the gas zone and the molten metal zone. O_2 enters this zone via lancing and diffusion from the gas phase (according to its partial pressure). The presence of iron oxides in the zone also increases the availability of oxygen for components with a sufficient reducing potential. Metallic elements (Fe, Mn, and Al) and nonmetal-

lic elements (C and Si) enter this phase from the molten-metal phase. Carbon is also added from injection and roof additions. Lime and dolime (CaO.MgO) added to the furnace are also included in this zone. All oxides accumulate in this zone, except for CO which leaves this zone and enters the gas phase as it is produced.

Molten-Metal Zone: Material enters this zone from the solid-scrap zone as it melts and leaves to enter the slag-metal zone according to the transport rate to the slag-metal interface.

It is assumed that no reactions occur in this zone because of the absence of O_2. Energy from the arc is added to the molten-metal and solid-scrap; energy is also transferred between the zones, driven by the prevailing temperature gradients. The presence of the following components are modelled in this zone: Fe, Mn, Al, Si, C. Mass transfer of material to the slag-metal zone is driven by natural diffusion, and also forced diffusion as a result of lancing.

Solid-Scrap Zone: The solid-scrap zone is modelled as a mass of steel that melts according to the quantity of energy transferred to it and the proximity of the steel temperature to its melting point. As steel liquefies it is removed from the solid steel zone and added to the molten steel zone. The model predicts a homogenous temperature in the solid-scrap zone, which corresponds to the average temperature of the scrap. However, in reality the temperature is not homogenous and scrap material melts continuously throughout the batch. This behavior is accounted for by dividing the available energy between sensible heating and melting according to the ratio of the steel temperature to its melting point.

The composite model comprises 85 differential, and 1,050 algebraic variables. A sensitivity analysis was carried out to identify a set of significant parameters whose values were, subsequently, estimated using eight batches of plant data. Details of the procedure followed are provided in MacRosty and Swartz.[12]

Formulation and Implementation of the EAF Optimization Problem

The profit per batch, in dollars, is

$$Z_P = c_0 M_{steel}(t_f) - \left(c_1 \int_0^{t_f} P\,dt + c_2 \int_0^{t_f} (F_{O_2,brnr} + F_{O_2,lnc})\,dt + c_3 \int_0^{t_f} F_{CH_4,brnr}\,dt + c_4 \int_0^{t_f} F_{C,inj}\,dt + c_5 \int_0^{t_f} F_{C,chg}\,dt + c_6 \int_0^{t_f} F_{flux}\,dt + c_7 \int_0^{t_f} (F_{scrap,1} + F_{scrap,2})\,dt \right) \quad (12)$$

where P is the electrical power; $F_{O_2,brnr}$ and $F_{O_2,lnc}$ are the flows of oxygen to the burner and from the lance respectively; $F_{CH_4,brnr}$ is the flow of natural gas to the burner; $F_{C,inj}$ and $F_{C,chg}$ are the carbon additions from injection and charging respectively; F_{flux} is the addition of lime and dolime; $F_{scrap,1}$ and $F_{scrap,2}$ are the rates of addition of the first and second scrap charges respectively; $M_{steel}(t_f)$ is the mass of liquid steel at the end of the heat (batch), and c_i is the associated unit cost of each component.

The optimization problem may be formulated according to different objective criteria, depending on the operational priorities of the plant personnel. Two such criteria involve optimization of the process according to the profit per time

$$\max_{\mathbf{u}(t),t_f} Z_{P/t_f} = Z_P\left(\frac{1}{t_f}\right) \quad (13)$$

and the profit per ton of liquid steel

$$\max_{\mathbf{u}(t),t_f} Z_{P/ton} = Z_P\left(\frac{1}{M_{steel}(t_f)}\right) \quad (14)$$

Using these different criteria to optimize operation may result in different operating policies, thus they should be applied in accordance with the plant operating mode and objectives. If the EAF is a bottleneck in the overall process operation, objective Eq. 13 would be appropriate, whereas objective Eq. 14 would be more suited to slow market conditions or if production is being delayed by a downstream unit. The control variables, $\mathbf{u}(t)$, in the optimization problem are P, $F_{O_2,brnr}$, $F_{CH_4,brn}$, $F_{O_2,lnc}$, $F_{C,inj}$ and $F_{scrap,2}$.

The dynamic optimization problem takes the form of Eqs. 1–6. The differential equations, Eq. 2, arise from the mass and energy balances, while the algebraic model equations, Eq. 3, are introduced from constitutive mass- and heat-transfer relationships, and the equilibrium conditions.

The commercial software gOPT/gPROMS[26] was used to solve the above problem. The software implements the sequential optimization approach, similar to the strategy outlined in Vassiliadis et al.[20] for the solution of DAE optimization problems. A discussion of the sequential approach was presented earlier. The DAE solver used for integrating the model and sensitivity equations implements a variable time step, backward differentiation technique; this implicit method is suitable for stiff systems. The optimization solver is an implementation of the sequential quadratic programming (SQP) algorithm, which is an effective strategy for the solution of nonlinearly constrained problems. SQP algorithms obtain the search direction based on the Hessian of the Lagrange function, or an approximation thereof, and a linear approximation of the constraints around the best current point.

An important consideration in solving these problems is that the nonlinear problem is nonconvex, and as a result, the search space may have multiple local optima. This can result in the optimization terminating at solutions that are not globally optimal. While there have been significant advances in the development of rigorous global optimization techniques, they are still limited to problems of relatively small dimension. A heuristic strategy employed to avoid obtaining a poor local solution is to restart the optimization from a range of different initial solutions to test if a better objective function value can be obtained.

Numerical robustness

A number of measures were employed to improve the numerical conditioning and to speed up the solution time of the optimization problem:

- Variable and equation scaling: Ensuring that all variables are of a similar order of magnitude and that the constraint equations are balanced relative to each other are well-

known strategies for improving the numerical conditioning of an optimization problem.

- Logarithmic transformations: The concentrations of certain components present in very small quantities may be driven to negative values during the course of the optimization. To address this, a logarithmic transformation was applied to the molar quantity at equilibrium, n_i by introducing a new variable n_i^L defined as

$$n_i^L = \ln(n_i) \tag{15}$$

The term, $e^{n_i^L}$ now replaces n_i in the formulation. The transformation avoids negative concentrations, and was found to improve the scaling of the problem, particularly when the equilibrium predicts very small concentrations of species.

- Discontinuous approximations: Model discontinuities were removed by approximating them with continuous functions, thereby allowing the gradient information to be successfully computed during optimization. More detail of the discontinuous approximation methods is given later.
- Solver integration tolerance: Lowering the integration tolerance greatly reduces the computational time for integrating the model equations. However, as the integration tolerance is decreased, the number of optimization iterations required to reach the optimum increases, because the accuracy of the sensitivity information is affected by the tolerance. Thus, there is a limit to the degree by which the integration tolerance can be lowered. Furthermore, if the integration tolerance is lowered beyond a certain point, the quality of the solution may become unacceptable.

Model discontinuities

The model includes a discontinuous element to deal with the fact that air may be sucked in or forced out of the furnace depending on the operation of the air handling system, the burner operation and the amount of gas being produced from the bath. Air being sucked in will have the composition of the ambient air, while air being expelled has the composition of the furnace freeboard. This behavior is readily captured during simulation by expressing the logical conditions through functions such as the max and min operators. However, the derivative discontinuity introduced by this type of expression poses a problem for gradient-based optimization algorithms. We observed in our application that as the optimal solution was approached, the condition number of the Hessian, used for optimization, deteriorated and as a result the optimization problem failed to converge. The poor conditioning could likely be attributed to a lack of derivative information of the discontinuous functions when constructing sensitivity information for the optimizer.

To handle this problem, the discontinuous function $g(x) = \max(0, f(x))$ is approximated by a continuously differentiable function[29]

$$g(x) = \frac{1}{2}f(x) + \frac{1}{2}(f(x)^2 + \varepsilon^2)^{\frac{1}{2}} \tag{16}$$

where a value of $\varepsilon = 1 \times 10^{-3}$ was found to be a good tradeoff between the sharpness of the approximation and degree of accuracy, and performed well. The inaccuracies that result from using this continuous approximation of the discontinuous function are negligible, particularly if one considers the amount of uncertainty associated with the prediction of the offgas flows and the air ingress into the furnace. Minimum functions are also easily handled since

$$\min(f(x), 0) = -\max(0, -f(x)) \tag{17}$$

Path constraints

In the control vector parametrization approach used, path constraints can be imposed on the states by adding point constraints at the control interval boundaries. This method ensures that constraints are satisfied at interval boundaries, but cannot guarantee that they are satisfied between the intervals; thus, small violations are possible. However, strict obedience of the constraints, $g(x) \leqslant 0$, can be ensured through the introduction of an endpoint constraint where the magnitude of the violation is integrated over the duration of the process and forced to be equal to zero. The integrated constraint violation is determined using the max operator

$$C_1 = \int_0^{t_f} [\max(g(x), 0)]^\gamma dt = 0 \tag{18}$$

The max operator can cause excessive oscillation between feasible and infeasible moves of the optimizer because when the constraint is inactive the violation measure and its gradient with respect to the control variables are zero. Vassiliadis et al.[30] advocate the use of both methods together as a hybrid approach to combine the exactness of the integral approach with the increased information regarding constraint location provided to the optimizer from the point constraints. They recommend using a value of $\gamma = 2$ since the function then has first-order continuity. However, in implementing these constraints it was found that using a value of $\gamma = 2$ as a general rule could result in failure of the optimization routine in cases where the initial solution had a large path constraint violation. The reason for the failure is attributed to the squared term which significantly increases the value of the constraint violation making it difficult for the optimizer to find a feasible solution. In this work, it was found that there was very little computational benefit gained by using values of $\gamma > 1$.

More recently, Chen and Vassiliadis[31] present an iterative method in which a sequence of optimal control problems is solved with an increasing number of inequality point constraints. The point constraints are added only in places along the horizon where violations are determined. The method is shown to converge within a finite number of iterations to a solution that satisfies the path constraints to any finite tolerance. Adding point constraints forces the integration algorithm to take small steps, and, therefore, this method avoids the problems associated with adding point constraints where they are not required.

Process Optimization Case Studies

A series of case studies is presented here; the purpose of these studies is to demonstrate how the fundamental model can be used within an optimization framework to improve profitability of the EAF process. An actual heat from the

industrial process on which the model parameters are based serves as the base case scenario for this study to illustrate typical furnace operation. The case studies are then presented to illustrate how optimization determines the economically optimal operating strategy of the furnace. The optimization problem is formulated such that the control variables may move between their upper and lower bounds in order to maximize the profitability of the heat (batch). The manipulated variables include the arc power, oxygen and natural gas flows to the burner, carbon injection, oxygen lancing, and the mass of the second scrap charge. The factors that are investigated include the cost of electricity, increasing the upper bound on the arc energy and consideration of the effect of batch duration on the profitability of operation.

The control vector **u**, was parameterized at 3-min intervals, except for those adjacent to the timing of the second scrap charge, so that this would coincide with an interval boundary. In Case Studies 1, 2 and 5, the control intervals were not allowed to vary. In Case 3, the final time is included as an optimization variable, and the last 5 control intervals were allowed to vary between 0–5 min. In Case 4, the first 5 intervals were fixed at 5 min, and the last 5 intervals were allowed to vary between 0–5 min; the final time was not a variable in this case.

Case 1: Optimal Solution

This case study investigates how the operation of the furnace may be improved by allowing the optimizer to determine the optimal manner of operation based on the economic objective function where the profit is maximized. The formulation of Eqs. 1–6 is used, where the elements of the control vector **u** are P, $F_{O_2,brnr}$, $F_{CH_4,brn}$, $F_{O_2,lnc}$, $F_{C,inj}$, $F_{scrap,2}$. The final time, t_f is assumed fixed in this case study, but is included in the optimization formulation in Case 3. The specific constraints imposed, in addition to the model equations, are

Input constraints:

$$P^{min}(t) \le P \le P^{max}(t)$$
$$F_i^{min}(t) \le F_i \le F_i^{max}(t)$$

Endpoint constraints:

$$m_{solid}(t_f) \le \varepsilon$$
$$y_{carbon}(t_f) \le Y_c^{max}$$

Path constraints:

$$T_{wall} \le T^{max}$$
$$V_{steel} \le V_{furnace}$$

The input constraints ensure that the flows and power addition are maintained within realistic bounds. The burner input flows are allowed to move between their upper and lower bounds except when the furnace is charged, at which time the maximum flow of the O_2 is decreased due to the roof being opened during this period; the flow of natural gas will be adjusted accordingly in the case of an economic objective and the upper bound is, thus, left unchanged. The initiation of carbon injection and the oxygen lancing is constrained by the fact that there needs to be a base of liquid steel before injection begins. The time of initiation of these flows, used in this case study, are the same as that used for the base case; however, the flows were allowed to fluctuate between maximum and minimum bounds. Providing an upper bound for the voltage tap as a function of the heat's progression is very complex since it can be affected by a number of factors that are not accounted for in the model. Examples of such factors include arc stability, collapsing of the scrap pile, and the electrodes arcing to the wall. Therefore, it was assumed that the power trajectory in the base case provides an upper bound on the power usage for the optimized case, with a lower bound of zero. The endpoint constraints ensure that all steel is melted, and that the carbon concentration is at the desired level. The path constraints maintain the wall temperature below its maximum bound and ensure that the maximum capacity of the furnace is respected when scrap is added.

Two scrap charges are considered, consistent with the industrial operation on which the studies are based. In all cases, the objective function given by Eq. 13 was used. In Case 1, the timing of the scrap charges was limited to the same as the base case, with the first charge added at time $t = 0$, and the second added at $t = 28$ min. The second charge is implemented by applying a rate of scrap input over a specific time interval. As was discussed previously, the rate of addition, and, hence, mass of the second charge, is a variable.

The optimal solution was determined, and improved profitability of the heat by 21% on a \$/time basis compared to the base case. The major improvement is realized through the optimizer determining the most efficient quantity and timing that material and energy are to be added during the heat. However, it should be noted that some of the improvement in this scenario will be due to fact that the optimizer can predict the exact conditions given by the model, whereas in reality, operators need to slightly overcompensate due to a lack of process data to ensure that endpoint conditions are met.

Figure 2 presents the offgas composition profiles for the base case and the optimal scenario, where the circles (o) and the crosses (×) represent the base case and optimal scenarios

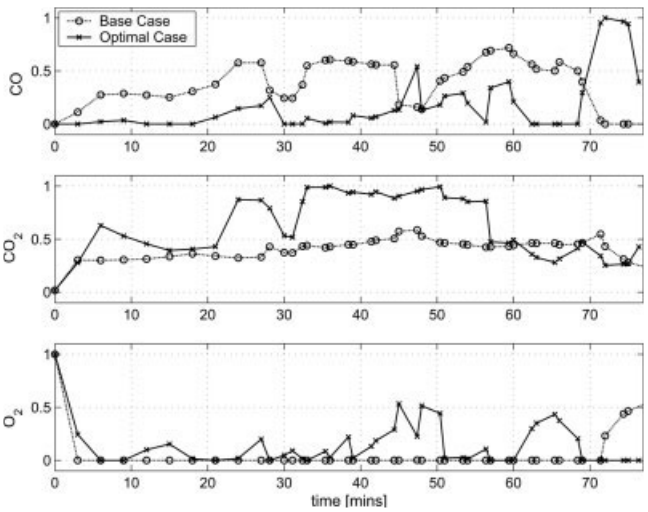

Figure 2. Case 1: Offgas data.

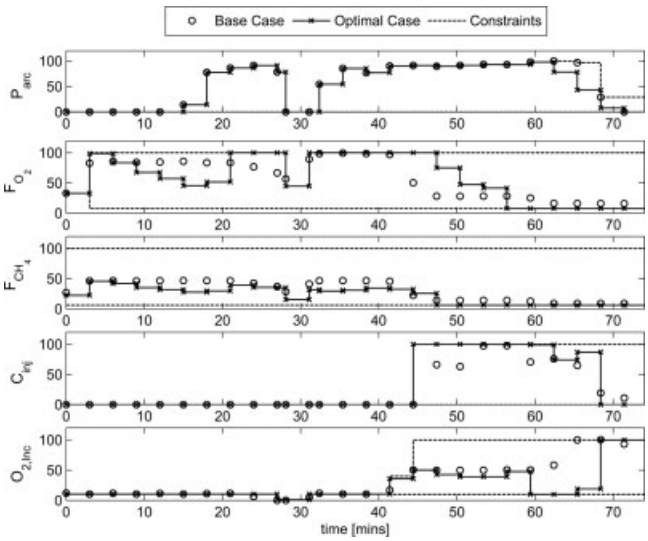

Figure 3. Case 1: Input profiles.

respectively. The data shown in this and the remaining case studies in this section have been scaled for proprietary reasons. In Figure 2, the mole fractions have been scaled relative to the maximum value of each component over the duration of the heat. From this figure it is apparent that much less CO is produced in the optimal scenario. The optimizer recognizes the energy potential of the CO, and, therefore, conserves CH_4 and combusts the CO instead. The net result is an economic saving due to the lower usage of CH_4, and also a cleaner and smaller volume of offgas. The model makes some assumptions with regard to the freeboard being a perfectly mixed reactor, therefore, this combustion could be more difficult to achieve in reality.

Figure 3 compares the scaled input profiles for the base case and the optimized case. The optimal solution indicates that slightly less power is used in the second charge; this energy is instead obtained from chemical sources. The F_{O_2} (burner oxygen) profile indicates a higher initial usage than the base case, and then steps down to a lower level as the batch progresses. This behavior is consistent with what is expected since the effect of the burners is related to the volume of solid scrap in the furnace. As melting occurs the effectiveness of the burners decreases, and, therefore, so should their usage. The sudden increase in the burner usage at approximately, $t = 22$ mins is due to a discrete carbon charge (in the form of coke) at approximately $t = 20$ mins. The purpose of the carbon addition is to create CO, which causes the slag to foam and also to provide a reducing agent to limit loss of iron to FeO. The complete combustion of CO to CO_2, known as post-combustion, is a valuable source of energy, and, thus, the optimizer puts the O_2 flow at its upper bound to maximize the use of this energy source. Studying the input profile for F_{O_2} from time $t = 45$–60 mins, it is evident that a higher amount of O_2 is needed in the furnace than was used in the base case scenario. The optimizer takes advantage of the fact that CO is again being produced from the bath due to lancing and harnesses this energy by increasing F_{O_2}. However, during the last stages of lancing ($t > 70$ min) the optimizer keeps the burner at its minimum level, even though there is a high presence of CO (see Figure 2) since there is no benefit gained from combusting this CO as all the steel is already at the required temperature. While it may be argued that it would be better to lance earlier, and, thus, harness this energy, this would result in production of more FeO thus impacting the yield. One could alternatively argue that more injection carbon could be added; however, this would be at an additional cost. This is a major benefit of using optimization with a fundamental model, since it is able to make these economic tradeoffs in determining the most profitable mode of operation.

Case 2: Cost of Power

In Ontario, Canada, the cost of power typically fluctuates between \$0.03–0.15/kWh throughout the day according to the grid demand, and has been known to reach \$0.50/kWh in extreme cases. The cost of other utilities, such as natural gas, oxygen and carbon are more stable, and fluctuate over much longer time horizons. Figure 4 is reproduced from data collected from the Independent Electricity System Operator (IESO),[32] and indicates the typical daily price fluctuations together with the demand in Ontario, Canada. As expected, the price is correlated with demand, and can, therefore, be predicted with some degree of certainty based on recent market trends and the time of day.

This case study investigates the impact that the cost of power has on the operation of the furnace. The time based objective function, given in Eq. 13, was again used, and the duration of the heat was fixed in these scenarios. Scenario A corresponds to optimal operation for an electricity cost of \$0.03/kWh. A second scenario (Scenario B) considers the case when the power cost is \$0.15/kWh. Figure 5 compares the input profiles of Scenarios A and B, which illustrates how the optimizer manipulates the operating strategy to compensate for the increased power cost. As expected, the optimizer attempts to reduce the amount of electrical energy used when the cost of power is higher; this is evident toward the end of the heat, after approximately 63 min. The opti-

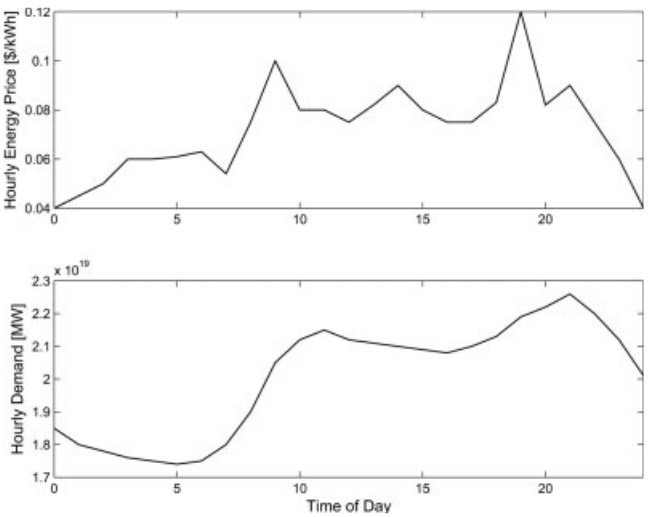

Figure 4. Hourly energy cost and demand for Ontario, Canada: March 10, 2005.

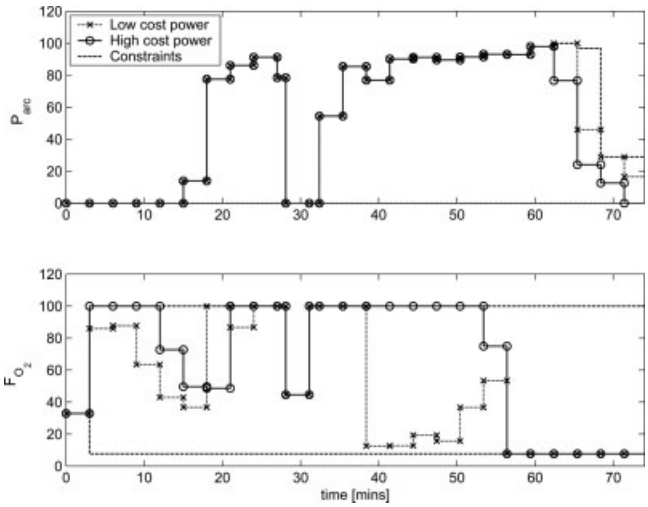

Figure 5. Case 2: Input profiles for comparing Scenarios A and B.

mizer compensates for the more expensive electrical power cost by substituting electrical power with chemical power, using a higher-burner flow in the initial 18 min, and again between $t = 39$–57 min.

A third scenario (Scenario C) considers a somewhat extreme situation, where the electricity cost is \$0.35/kWh. The value of the objective functions for each case is reported in Table 1. The values are reported relative to the base case for proprietary reasons; they have been normalized by dividing by the profit for the base case study and multiplying by 100. Thus, numbers larger than 100 indicate batches which are more profitable than the base case and numbers less than 100 are less profitable; note the power cost in the base case was \$0.05/kWh. Negative values indicate batches that would operate at a loss. The optimal solution was determined at each of the given power prices; these numbers are reported in bold in the table. The objective function was then evaluated for each of the other power costs using the same input trajectories, which corresponds to the other values reported in the same row in the table. The number in bold has the highest value in the column, which is expected since the input profiles have been optimized at that particular value of the cost of power. We also observe that the input trajectories that are optimal for electricity costs of \$0.05/kWh and \$0.03/kWh result in a loss if the electricity cost increases to \$0.35/kWh. However, profitable operation at this high electricity cost is achievable using trajectories that are optimal for higher electricity prices of \$0.15/kWh and \$0.35/kWh.

Studying the data in the table it appears that while there are benefits to be gained from optimizing the operating practice when the power cost is low, greater benefits in changing the operating practice would be realized as the power cost increases to \$0.15/kWh and above. This case study motivates modifying the operating practice based on the current power costs. The results from these studies indicate that shifting the current practice to favor increased burner usage during peak demand times and scaling back again as the power cost drops would result in increased profitability.

Table 1. Comparison of Profit Based on Power Cost Relative to Base Case

Case Study	\$0.05/kWh (\$/min)	\$0.03/kWh (\$/min)	\$0.15/kWh (\$/min)	\$0.35/kWh (\$/min)
1	**122.5**	129.8	81.9	−17.9
2A	122.1	**130.2**	80.6	−5.1
2B	122.0	129.3	**83.0**	2.3
2C	120.4	128.0	82.4	**6.5**

The majority of EAF operations are mostly controlled by the operators who aim to achieve consistency from batch to batch through repeating the same operating practice. Taking this into consideration, it may be desirable to encourage the night-shift operators to follow an operating practice determined from optimizing at a low power cost, and to give the day-shift operators an operating practice determined at a moderate power cost. This averaging strategy would theoretically be less effective than considering the current power levels and changing the practice every heat, but considering that EAFs involve minimal automation, and are still predominantly run by operators, it would likely yield improved overall performance over current practice.

Case 3: Increased Upper Bound on Power Input

The purpose of this case study is to increase the bound on the maximum power by 20% after the second charge, and include the end time as a variable in the optimization problem. This study illustrates the potential benefits that may be gained from using a higher tap setting on the transformer, or equivalently, the potential benefits that may be obtained from purchasing a transformer with a higher rating if current practice is limited by the maximum tap setting available. It is possible that this mode of operation may not be realizable in practice as other factors not accounted for in the model might place more stringent constraints on the power input.

The optimization was carried out using the form of the objective function given in Eq. 13, and in this case study the duration of the heat was included as an optimization variable. The input trajectories for this case study are shown in Figure 6. The most interesting variable is the arc power, which appears to favor operating at its upper bound until about

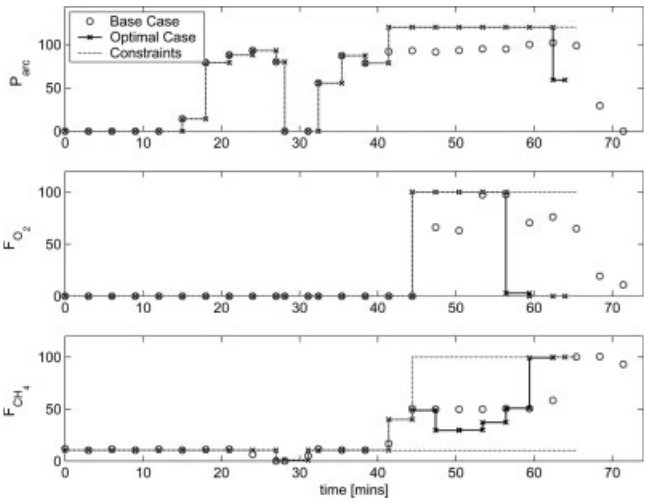

Figure 6. Case 3: Input profiles.

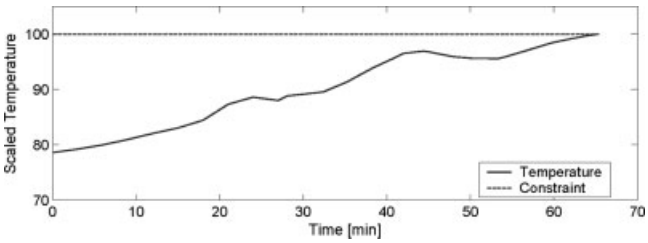

Figure 7. Case 3: Wall temperature.

62 min into the heat when it retreats for the last several minutes of the heat. The temperature profile for the wall is shown in Figure 7. The furnace wall temperature imposes a constraint on the operation of the furnace. Good foaming between 45 and 55 min prevents the wall temperature from escalating even though the power input remains at the upper bound. However, after 55 min as the oxygen lancing increases and the carbon in the bath is exhausted the foaming decreases and the wall temperature begins to increase. This, consequently, requires the power to be reduced to prevent the wall temperature from violating the constraint at the end point. If this temperature bound were not present, the solution would require much less foaming to protect the walls, and the heat would be marginally shorter since it would not have to reduce the power level during the final stages. The amount of power and burner fuel used in this case study was more than was required in Case 1. However, the profit obtained for this study was much greater than Case 1, due chiefly to the reduction in the duration of the heat by several minutes. The normalized profit was \$138.2/min in this case compared to \$122.5/min in Case 1.

This case indicates that there may be significant benefit to increasing the upper bound on the power input when the end time is a variable, particularly if a higher production rate is desirable. During times when the steel market is good and high-throughput rates are desirable, this approach does provide some promising opportunities. However, during market slumps when the steel price is low and inventories are near capacity, throughput rates are not a concern. During such periods it would not be desirable to follow the strategies advocated in this particular case study since the cost per ton of liquid steel is greater, due to the larger quantities of power and burner fuel utilized in reducing the heat time. Evidence of the higher cost is provided in Table 2, which compares the normalized profits from case studies 1 and 3 on a per time, and a per ton of liquid steel basis.

Case 4: Fixed Preheat Duration

The furnace preheat is the time before the power is switched on, when the only external source of heating is from the burners. In this case study, a fixed amount of time is made available for the preheat; however, the furnace is not required to use the burners during this period. The case study simulates the situation of a twin shell operation that shares a single transformer and set of electrodes. This is a fairly common industrial installation, consisting of two furnaces which operate sequentially; while the electrodes are being used on one furnace, the second furnace will be charged and then preheated. In this case study, the time based objective function given in Eq. 13 was again used and the batch duration was fixed.

Table 2. Comparison of Profit for Cases 1 and 3 Relative to Base Case

Case Study	\$/min	\$/ton
1	122.5	107.8
3	138.2	105.1

In the base case scenario, the preheat time was approximately 15 min; in this case the time available for preheating is extended to 25 min. At time zero the furnace will have a 20 ton hot heel, and 122 tons of cold scrap. Figure 8 shows the optimal power and burner input profiles as determined for this case.

As expected, the solution does not keep the burners on for the full time period available for the preheat. The reasons for this are twofold: first, the burners will be most efficient when the scrap is cold, and second, overuse of the burners decreases the overall yield due to the oxidation of the steel.

A surprising result is that the burner operation is initiated from $t = 0$ and heats up the scrap for a period of 5 min, then allows it to cool for approximately 15 min before being turned on 5 min prior to the power being started. This counterintuitive result is explained by the fact that the hot heel is also present from the initial point and loses heat to the cold scrap and furnace over the duration of the 25-min period. The heel, however, transfers heat much more effectively to the scrap than the burner, since the transfer takes place via radiation and conduction as opposed to convective transfer in the case of the burner. Furthermore, the energy in the heel is a more valuable energy source than the burners since it can overcome the latent heat of fusion to melt the solid scrap. At time $t = 0$, there exists a large difference between the temperature of the heel, and the temperature of the scrap and furnace walls resulting in large amounts of energy being transferred from the heel to the solid scrap. As energy leaves the heel it cools and, subsequently, its ability to melt the scrap diminishes. Starting the burner early takes advantage of the fact that heat transfer from the burners is most efficient

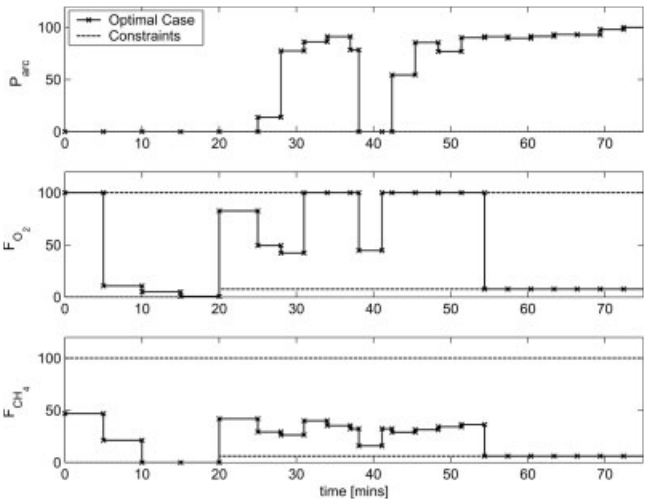

Figure 8. Case 4: Comparison of inputs.

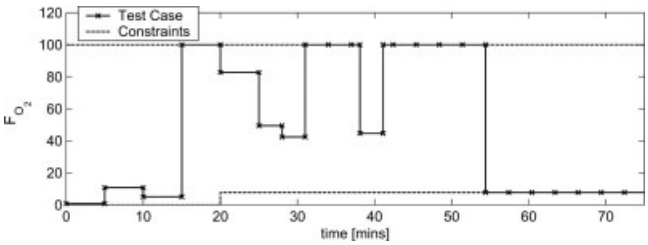

Figure 9. Case 4: Burner input for test case.

when the scrap temperature is low, and also preserves more of the valuable energy in the heel by reducing the temperature difference between the scrap and the heel; more energy is, thus, available in the heel for sensible heating above the range of the burners, and also for overcoming the latent heat of fusion. Thus, the net effect of starting the burner at time $t = 0$ more than compensates for the cooling that occurs while the burner is switched off.

To verify this result the optimal solution was simulated again except the burner action specified for the first interval was shifted later to time $t = 15$ min, as shown in Figure 9. The results from the simulation revealed that the heat was not able to meet the endpoint conditions in this case and melt all the scrap material by the final time. This is a significant result because it shows that the timing of the burner operation, and not just the duration are important when long periods are available for preheating.

Case 5: Event-activated Constraint Formulation

In the previous case studies, the manner in which the oxygen lancing and carbon injection bounds were formulated in the optimization problem was determined from the base case operation. Approximately 44 min after the initiation of the heat, the upper bound was relaxed and the lance/injection rate was allowed to increase to the actuator limit. However, in industry, the plant operators typically begin active lancing, that is, increasing the flow from its lower bound, once the cumulative power input has exceeded a predetermined threshold, which for the industrial operation under consideration is 50MWh. The cumulative power input into the furnace is used as an indicator variable to determine when lancing may begin. This case investigates a better method of constructing the upper bound for oxygen lancing, and carbon injection by relating it to the cumulative power input instead of time. The time based objective function, given in Eq. 13 was used for the scenarios in this case study and the batch duration was fixed.

Two methods for formulating this constraint are presented here, the first of which is a more direct representation, and can be used with any type of objective function. The second formulation yields a more efficient solution, and is valid when an economic criterion is used as the objective function. The formulation development is shown only for oxygen lancing since the carbon injection formulation is analogous.

A strategy to allow constraints to move along the horizon independently of the intervals was implemented, that uses a hyperbolic tangent switching function to limit the flow rate to the minimum flow until the cumulative total power, $\int_0^t P_T dt'$, exceeds 50MWh, after which the upper bound is increased to the maximum actuator value. This was formulated as

$$W = \frac{1}{2}\tanh\left[\gamma\left(\int_0^t P_T dt' - 50\right)\right] + \frac{1}{2} \tag{19}$$

$$F^{\max}_{lance,O_2} = (F_A^{\max} - F_A^{\min})W + F_A^{\min} \tag{20}$$

where W is the switching variable between 0 and 1, and γ is a factor that controls the rate of switching. The term, $(\int_0^t P_T dt' - 50)$, forces W to switch when the cumulative total power reaches 50 MWh. $F^{\max}_{lance,O_2}$ is the upper bound for the lance oxygen, and $F_A{}^{\max}$ and $F_A{}^{\min}$ are the maximum and minimum actuator values, respectively. It is important to formulate the problem so that the upper bound reduces to a minimum bound and not zero, since during the heat a minimum flow level must be maintained to prevent blockages from slag or molten metal solidifying in the nozzle.

In addition to the actuator constraints, the flow must be less than or equal to the upper bound

$$F_{lance,O_2} \le F^{\max}_{lance,O_2}. \tag{21}$$

Figure 10 illustrates the application of the switching function described by Eq. 19 for $\gamma = 50$, which forces the switch to be very sharp. Shown in this figure is the upper bound as determined in Eq. 20, together with the actuator bounds. The inclusion of Eq. 21 forces the minimum actuator bound to be followed while the cumulative power is less than 50MWh. Once the energy level has been exceeded the lance flow is free to move between the original limits.

The input constraint is converted to an endpoint constraint in the formulation to allow it to be enforced over the time horizon. This is accomplished through the introduction of the following equations;

$$\frac{d}{dt}(F^M_{lance,O_2}) = \max(0, F_{lance,O_2} - F^{\max}_{lance,O2}) \tag{22}$$

$$F^M_{lance,O_2}(t_f) \le \varepsilon. \tag{23}$$

$F^M_{lance,O_2}(t)$ is a variable introduced to track the accumulation of the violation. This formulation was found to result in convergence difficulties unless a good starting point was provided to the optimizer.

Thus, an alternative method for handling the event-activated constraint was formulated. In this formulation a new variable, F^*_{lance,O_2}, is introduced that will be manipulated by the optimizer between the actuator limits

$$F_A^{\min} \le F^*_{lance,O_2} \le F_A^{\max} \tag{24}$$

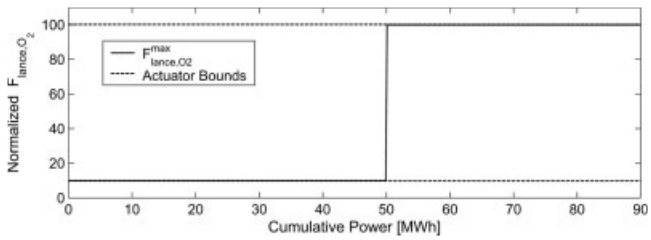

Figure 10. Event-activated constraint.

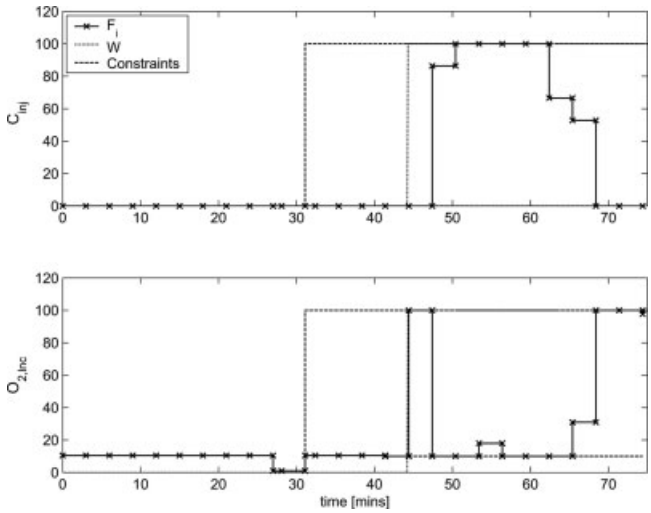

Figure 11. Case 5A: Event-activated constraint.

The lance oxygen flow rate that actually enters the furnace, F_{lance,O_2}, is related to this new variable as follows,

$$F_{lance,O_2} = \left(F^*_{lance,O_2} - F_A^{\min}\right)W + F_A^{\min} \tag{25}$$

W is the switching variable and when equal to 1, then $F_{lance,O_2} = F^*_{lance,O_2}$, and, thus, the value of the flow rate chosen by the optimizer corresponds to the value fed into the furnace. However, when $W = 0$ then $F_{lance,O_2} = F_A^{\min}$ and the value of F^*_{lance,O_2} is free to take on any value in the range given in Eq. 24. The integrity of this formulation is maintained for an objective that minimizes cost or maximizes profit. With the new variable F^*_{lance,O_2}substituted into the cost function in place of the original variable, F_{lance,O_2}, the equality, $F_{lance,O_2} = F^*_{lance,O_2}$, is again enforced due to the economic penalty that would otherwise be incurred for material that cannot be used.

In Case 5A. the constraint was triggered at 50MWh. The objective function obtained from using this formulation is comparable to that obtained in Case 1; the normalized objective value was \$122.1/min in this case compared to \$122.5/min in Case 1. The slight difference is expected because the optimal time initiation of injection and lancing is not expected to coincide exactly with 50MWh; in fact the base case allowed injection to begin at an accumulated power input of just 46.8MWh. This constraint formulation encourages more energy to be put into the furnace earlier in order to reach the 50MWh constraint and initiate lancing sooner; resulting in a slight variation in the strategy compared to that of Case 1. Figure 11 illustrates the lancing and injection profiles together with their upper and lower bounds; the switching variable W is superimposed over the figure to illustrate the activation of the constraint. The lance injection begins as soon as the cumulative power reaches 50MWh.

This formulation was less efficient, from a computational viewpoint, than formulating the problem with the constraint bounds tied directly to the time intervals, as was done in Case 1. The optimization problem took 44 iterations, and 4613 CPU s to solve on a Intel Pentium IV 3.0 GHz processor, compared to 28 iterations and 2830 CPU s for Case 1.

In Case 5B, the cumulative power at which the switching function was triggered was included as an optimization variable. Eq. 19 is modified as follows

$$W = \frac{1}{2}\tanh\left[\gamma\left(\int_0^t P_T dt' - P_{switch}\right)\right] + \frac{1}{2} \tag{26}$$

where P_{switch} is now a variable included in the optimization problem. The results of this scenario indicated that initiating lancing after 44.9MWh of energy have been added to the system was optimal, giving an objective function value of 122.6 compared to 122.5 in Case 1. This formulation took 6001 CPU seconds and 64 NLP iterations to converge.

Comparison of scenarios

Table 3 summarizes the profit per minute, yield, the cumulative power input and cumulative oxygen burner flow for each case. A column indicating whether final time was included as an optimization variable in the formulation is also shown. The values have been normalized relative to the base case, but the units of the original variables are reported as a source of reference.

Comparing results between the base case and Case 1, the main difference is the more efficient use of the material and power additions. The second case study illustrates the intuitive result that a higher electricity price favors a decrease in power usage and a greater reliance on burner energy. A greater loss of Fe to FeO is observed when the burner is more heavily utilized; evidence of this is seen by comparing the steel yields for scenarios A and B presented in the second case study. The third case study takes advantage of the relaxed upper bound on power input to improve profitability by reducing the processing time. Case 4 differed from the other scenarios in that an extended period of time of preheating was forced to occur. This study showed some interesting results as it forced the burner to come on early to maximize its benefit by heating the scrap and thereby preserving the more valuable energy in the heel. The strategies obtained in Case 5 and Case 1 were very similar; however, Case 5A shows a slight increase in power usage, and also a slightly smaller profit. The differences are expected due to the difference in the formulation of the problem. The increase in power consumption in Case 5A is likely a result of the optimizer trying to force lancing to happen as soon as possible by increasing the power input so that the cumulative power exceeds 50MWh sooner. In Case 5B, the cumulative power

Table 3. Summary of Case Studies Relative to Base Case

	Profit $\left[\frac{\$}{\text{min}}\right]$	Yield [%]	$\int P$ [MWh]	$\int O_2$ $[m^3_N]$	t_f (Y/N?)
Base case	100.0	100.0	100.0	100.0	N
Case 1	122.5	101.5	93.3	90.9	N
Case 2A	130.2	101.5	97.5	77.0	N
Case 2B	83.0	100.8	91.9	102.1	N
Case 2C	6.5	100.8	90.7	107.3	N
Case 3	138.2	100.9	100.2	96.3	Y
Case 4	107.2	102.2	105.9	70.3	N
Case 5A	122.1	101.5	94.1	87.0	N
Case 5B	122.6	101.5	93.4	91.1	N

value at which the switch occurs was included as an optimization variable; the optimal operating strategy closely mimics that of Case 1 although a small improvement is realized from initiating lancing earlier, at 44.9MWh instead of at 46.8MWh as was the case for Case 1.

Each of the optimization case studies takes approximately an hour to run on an Intel Pentium IV 3.0 GHz processor, where approximately 85% of the CPU time is spent on the integration of the sensitivity equations. The actual time in each case depends on the proximity of the initial solution to the optimum, as well as the particular case being studied. In cases where time is included as a variable in the optimization problem, the solution time was observed to be much longer, approaching 2 h. The likely reason for this observation is the increasing complexity of the problem due to the interaction of the free end-time and determination of the control variables, which likely causes the non-linearity and nonconvexity of the problem to worsen. The increase in the number of optimization variables is also a factor.

Summary and Discussion

An EAF optimization formulation was presented, and its flexibility and potential for process improvement illustrated through several case studies. Analysis of the results reveals that by optimization of a detailed process model, tradeoffs inherent in the EAF process operation can be quantitatively accounted for.

At the current state of the model, the optimization serves as a very useful tool for ascertaining the impact on profitability of the various inputs, and steering the process toward more profitable operation. Already, case studies presented here have been used by plant personnel to both motivate and design plant trials. Furthermore, the case studies illustrated here demonstrate the potential benefit of optimization, and motivate both further development of the model and also investment in measurement systems for the collection of more data.

The data that were available for estimation for the model resulted in a fair amount of model uncertainty, and, thus, it is not possible to guarantee that the improvements represented in Table 3 would be realized on the actual process through the implementation of the respective strategy. However, the strategies advocated indicate the direction in which the process should be moved in order to improve profitability and the corresponding trade-offs that are made.

In this work, plant-model mismatch and disturbances are not considered in determining the optimal profiles, both of which may cause the nominal optimal solution to be suboptimal or infeasible when implemented. A preliminary investigation into the incorporation of a feedback strategy to compensate for the effects of such model uncertainty has been conducted, with promising results. Planned future work includes the development of reduced order models, suitable for on-line application.

Acknowledgments

The authors gratefully acknowledge valuable input from Michael Kempe and Stephen Waterfall of Dofasco. Funding for this work was provided by the McMaster Steel Research Centre, Materials and Manufacturing Ontario, and the McMaster Advanced Control Consortium.

Literature Cited

1. Fruehan RJ. *The Making, Shaping and Treating of Steel*. 11th ed. Pittsburgh, PA: AISE Steel Foundation; 1998.
2. Irons GA. Developments in electric furnace steelmaking. In: *AIS-Tech 2005*. Charlotte, NC; 2005.
3. Woodside CM. Pagurek B, Paukens J, Ogale AN. Singular arcs occuring in optimal electric steel refining. *IEEE Trans Automat Contr*. 1970;AC-15:549–556.
4. Gosiewski A, Wierzbicki A. Dynamic optimization of a steel-making process in electric arc furnace. *Automatica*. 1970;6:767–778.
5. Görtler G, Jörgl P. Energetically optimized control of electric arc furnace. In: *Proceedings of the 2004 IEEE International Conference on Control Applications*. 2004;137–142.
6. Oosthuizen DJ, Craig IK, Pistorius PC. Economic evaluation and design of an electric arc furnace controller based on economic objectives. *Control Eng Practice*. 2004;12:253–265.
7. Boemer A, Roedl S. Optimisation of the electric arc furnace lancing strategy by physical and numerical simulation. *Steel Res*. 2000;71: 197–203.
8. Pozzi M, Maiolo J, Memoli F. EAF process optimisation with Techint Technologies. *Steel Times International*. 2005;24:20–22.
9. Jones J. Safe P, Wiggins B. Optimization of EAF operations through offgas system analysis. In: *58th Electric Furnace Conference Proceedings*. Warrendale, PA: ISS Publishers; 1999.
10. Maiolo JA, Evenson EJ. EAF performance analysis and optimization – A statistical approach. In: *Proceedings of the Gerald Heffernan International Symposium on Innovative Technologies for Steel and Other Materials*. Toronto, Canada; 2001;109–123.
11. Matson S, Ramirez WF. Optimal operation of an electric arc furnace. In: *57th Electric Furnace Conference Proceedings*. Warrendale, Pennsylvania: ISS Publishers; 1999;719–728.
12. MacRosty RDM, Swartz CLE. Dynamic modeling of an industrial electric arc furnace. *Ind Eng Chem Res*. 2005;44:8067–8094.
13. Cervantes A, Biegler LT. Optimization strategies for dynamic systems. In: Floudas CA, Pardalos PM, eds. *Encylcopedia of Optimization*. Dordrecht, The Nethelands: Kluwer Academic Publishers; 2001;4:216–227.
14. Pontryagin LS, Boltyanskii VG, Gamkrelidze RV, Mishchenko EF. *The Mathematical Theory of Optimal Processes*. New York: Interscience Publishers Inc; 1962.
15. Biegler LT, Grossmann IE. Retrospective on optimization. *Comput Chem Eng*. 2004;28:1169–1192.
16. Cuthrell JE, Biegler LT. On the optimization of differential-algebraic process systems. *AIChE J*. 1987;33:1257–1270.
17. Cervantes A, Biegler LT. Large-scale DAE optimization using simultaneous nonlinear programming formulations. *AIChE J*. 1998; 44:1038–1050.
18. Biegler LT, Cervantes AM, Wächter A. Advances in simultaneous strategies for dynamic process optimization. *Chem Eng Sci*. 2002; 57:575–593.
19. Hong W, Wang S, Li P, Wozny G, Biegler LT. A quasi-sequential approach to large-scale dynamic optimization problems. *AIChE J*. 2006;52:255–268.
20. Vassiliadis VS, Sargent RWH, Pantelides CC. Solution of a class of multistage dynamic optimization problems. 1. Problems without path constraints. *Ind Eng Chem Res*. 1994;33:2111–2122.
21. Bock HG, Plitt KJ. A multiple shooting algorithm for direct solution of optimal control problems. In: *Proceedings of the 9th IFAC World Congress, Budapest*. Pergamon Press; 1984;1603–1608.
22. Santos LO, de Oliveira NMC, Biegler LT. Reliable and efficient optimization strategies for nonlinear model predictive control. In: Rawlings JB, ed. 4th *IFAC Symposium on Dynamics and Control of Chemical Reactors, Distillation Columns and Batch Processes, DYCORD+'95*. Danish Automation Society; 1995;33–38.
23. Leineweber DB, Bauer I, Bock HG, Schlöder JP. An efficient multiple shooting based reduced SQP strategy for large-scale dynamic process optimization. Part 1: theoretical aspects. *Comput Chem Eng*. 2003;27:157–166.

24. Bellman RE, Dreyfus SE. *Applied Dynamic Programming*. Princeton, NJ: Princeton University Press; 1962.
25. Kirk DE. *Optimal Control Theory. An Introduction*. Englewood Cliffs, NJ: Prentice-Hall; 1970.
26. Process Systems Enterprise Ltd. *gPROMS Advanced User Guide. Version 2.3;* 2004.
27. Cameron A, Saxena N, Broome K. Optimizing EAF operations by dynamic process simulation. In: *56th Electric Furnace Conference Proceedings*. Warrendale, Pennsylvania: ISS Publishers; 1998;689–696.
28. Smith WR, Missen RW. *Chemical Reaction Equilibrium Analysis*. New York: Wiley; 1982.
29. Biegler LT. Personal Communication; 2004.
30. Vassiliadis VS, Sargent RWH, Pantelides CC. Solution of a class of multistage dynamic optimization problems. 2. Problems with path constraints. *Ind Eng Chem Res*. 1994;33:2123–2133.
31. Chen TWC, Vassiliadis VS. Inequality path contraints in optimal control: A finite iteration ε-convergent scheme based on pointwise discretization. *J Proc Contr*. 2005;15:353–362.
32. Independent Electricity System Operator (IESO). http://www.ieso.ca/; 2005.

Manuscript received July 28, 2006, and revision received Dec. 12, 2006.